Available online at website: https://journal.bcrec.id/index.php/bcrec

Bulletin of Chemical Reaction Engineering & Catalysis, 21 (3) 2026, 710-716

Original Research Article

Cation-dependent Behavior of Aluminium under Pulsed Electrolysis

Marina Kubanova, Tatyana Yureva, Elena Yatsenko, Yash V. Kataria*, Alexandra Kuriganova, Mikhail Lipkin, Nina Smirnova

Department of Technology, Platov South-Russian State Polytechnic University (NPI), Novocherkassk 346428, Russia.

Received: 8th May 2026; Revised: 19th June 2026; Accepted: 19th June 2026
Available online: 23th June 2026; Published regularly: October 2026

Abstract

For decades, chloride ions Cl^- have been considered a key factor in the electrochemical behavior of aluminum in chloride electrolytes, including depassivation, pitting corrosion, and anodic dissolution. However, the influence of electrolyte cations has been considered secondary or ignored in most classical studies. In this study, we investigated the influence of electrolyte cations ($MgCl_2$, $CaCl_2$, $SrCl_2$, $BaCl_2$) on the electrochemical behavior of aluminum under the influence of an alternating symmetrical pulsed current with a density of 1 $A.cm^{-2}$. The study found that in the presence of Ba^{2+} and Sr^{2+}, aluminum is oxidized to form dispersed two-phase products AlOOH and $Al(OH)_3$, with an average particle size of 1.9 and 2.2 nm for the AlOOH phase and 20.4 and 13.9 nm for the $Al(OH)_3$ phase. In Mg^{2+} and Ca^{2+} chlorides, passivating films of $Mg(OH)_2$ or $Ca(OH)_2$ are formed, as well as layered double hydroxides – $Mg_6Al_2(OH)_{16}Cl_2{\cdot}4H_2O$ (*Mg-Al* LDH) or $Ca_2Al(OH)_6Cl{\cdot}2H_2O$ (*Ca-Al* LDH), respectively, which inhibit aluminum corrosion under pulse electrolysis conditions, even in the presence of activating Cl^- ions.

Keywords: Aluminium; alkaline earth metal cations; alternating pulsed current; corrosion; passivation

How to Cite: Kubanova, M., Yureva, T., Yatsenko, E., Kataria, Y. V., Kuriganova, A., Lipkin, M., Smirnova, N. (2026). Cation-dependent Behavior of Aluminium under Pulsed Electrolysis. *Bulletin of Chemical Reaction Engineering & Catalysis*, 21 (3), 710-716. (DOI: 10.9767/bcrec.20728)

Permalink/DOI: https://doi.org/10.9767/bcrec.20728

1. Introduction

Recent comprehensive studies in the electrochemistry of aqueous solutions have been motivated by practical concerns, such as hydrogen production [1,2] and the utilization of aqueous electrolytes in electrochemical energy storage systems that have conventionally employed non-aqueous electrolytes [3,4], as well as fundamental challenges, including the elucidation of structural properties. The production of insoluble compounds on the electrode surface may block the target electrochemical process and prolong the effective range of electrolyte voltage stability beyond the thermodynamic limit [5-7].

An intriguing research domain is the behaviour of the electrode-electrolyte interface under pulsed electric fields in aqueous electrolytes, characterized by frequent reversals of electrode polarity, resulting in a continual alteration of the electrical double layer's structure. This study examined the behavior of aluminium in aqueous solutions of alkaline earth metal chlorides under symmetrical pulsed alternating current (PAC). The interest in aluminium arises from the formation of a thin layer of Al_2O_3 on its surface upon exposure to air, especially in aqueous solutions, leading to markedly different electrochemical behavior at the metal oxide-H_2O interface compared to the metal-H_2O interface.

The utilization of pulsed electric fields in an electrochemical system arises from the potential to produce a range of beneficial dispersion products [8-12]. The passivity of aluminium in aqueous electrolytes can be mitigated by employing Cl^- anion-containing electrolytes, as demonstrated by numerous researchers [13]. Additionally, the application of pulsed electrolysis to aluminium in these electrolytes, including

* Corresponding Authors.
Email: katariayash1603@gmail.com (Y.V. Kataria)

those based on monovalent cations, facilitates the production of dispersed $Al(OH)_3$/AlOOH products [14], which can be used as catalyst carriers [15]. But what about other divalent alkaline earth cations? Divalent alkaline earth cations Mg^{2+}, Ca^{2+}, Sr^{2+} and Ba^{2+} exhibit superior mobility compared to Na^+ [16], resulting in enhanced electrical conductivity of the electrolyte solution. This phenomenon theoretically facilitates the kinetics of dispersed Al-based product formation under pulsed electrolysis conditions and may influence their composition and microstructure, as demonstrated in the case of zinc [16].

This study proved the substantial impact of divalent electrolyte cations (Mg^{2+}, Ca^{2+}, Sr^{2+} and Ba^{2+}) on the electrochemical behavior of aluminium under the application of alternating pulsed current in the electrochemical system. The data acquired could in turn establish a foundational comprehension of the electrochemistry of valve metals influenced by pulsed electric fields.

2. Materials and Methods

The behaviour of aluminium in response to PAC was examined in 1 mol.L^{-1} chloride electrolyte solutions (Mg^{2+}, Ca^{2+}, Sr^{2+}, Ba^{2+}). Pulse electrolysis was carried out in a four-electrode electrochemical cell with a pulsed alternating current source with a frequency of 50 Hz, as detailed in [14]. Aluminium plates (99.5%) of identical area were utilized as working electrodes. A symmetrical pulsed current with an average anodic to cathodic average current density ratio of j_a:j_k= 1:1 A.cm^{-2} was applied to the electrodes. Electrolysis was carried out with constant stirring (300 rpm) and a temperature of 60±2 °C.

The rate of electrolysis products formation (W) was determined by the formula:

$$W = \frac{\Delta m_{Al}}{S_{Al}\tau} \quad (1)$$

where Δm_{Al} – difference between the mass of aluminium electrodes before and after electrolysis, S_{Al} – geometric area of aluminium electrodes, τ – duration of electrolysis.

Polarization experiments, (cyclic voltammetry and chronopotentiometry) were conducted in a three-electrode electrochemical cell at a temperature of 20±10 °C with an Elins P-45X potentiostat. A platinum electrode functioned as the counter electrode, while a saturated Ag/AgCl electrode acted as the reference electrode. Electrochemical impedance spectroscopy was conducted in potentiostatic mode using an alternating current signal sweep amplitude of 10 mV throughout a frequency range of 10^{-1}–10^5 Hz. The impedance measurement data were estimated with ZView software.

X-ray diffraction (XRD) studies were conducted utilizing an ARL X'TRA X-ray diffractometer (Thermo Fisher Scientific Inc., USA) employing Cu-Kα radiation (λ = 1.5406 Å). XRD patterns were obtained in continuous-scanning mode with a 2θ range of 15° to 130°, at an interval of 0.02 s and a speed of 3° min^{-1}. The resolution function of the diffractometer was established utilizing NIST powder LaB_6 (NISTSRM660a).

3. Results and Discussion

A white precipitate developed in the electrolyte upon the application of an alternating pulse current with a profile presented in Figure 1a to the aluminium electrodes. The cationic composition and concentration of the electrolyte influenced the accumulation rate of this precipitate (Table 1). In electrolytes containing

Table 1. Electrochemical parameters of Al-based electrochemical system in dependence on electrolyte cation.

Parameter		Cation			
		Mg^{2+}	Ca^{2+}	Sr^{2+}	Ba^{2+}
Rate of aluminium electrode dispersion under PAC, mg.cm^{-2}.h^{-1}		-	-	150	148
pH electrolyte under PAC		3.8	4.3	9.8	10.0
Potential pause after pulse, V	cathodic	-1.52	-	-1.70	-1.50
	anodic	-0.96	-	-1.18	-1.18
Chronoamperometry	Time of relaxation, sec	80	53	5	5
	E_{an}, V at j = +10 mA.cm^{-2}	-0.75	-0.74	-0.75	-0.74
	E_{cat}, V at j = -10 mA.cm^{-2}	-1.9	-1.6	-1.5	-1.4
Tafel plot	b_{an}, mV.dec^{-1}	57	55	45	47
	b_{cat}, mV.dec^{-1}	-57	-45	-35	-42
	$logj_{corr}$, A.cm^{-2}	-5.9	-5.8	-5.8	-5.7
	E_{corr}, V	-1.30	-1.34	-1.12	-1.07
EIS	*R1*	0.5365	10.42	0.2232	0.7498
	R2	$4.8 \cdot 10^9$	$3.09 \cdot 10^9$	$4.9 \cdot 10^{-9}$	$6.69 \cdot 10^{-9}$
	CPE	$1.95 \cdot 10^{-5}$	$3.73 \cdot 10^{-5}$	$5.007 \cdot 10^{-6}$	$1.618 \cdot 10^{-5}$

Sr^{2+} and Ba^{2+} an accumulation rate of dispersed products was about 150 mg $cm^{-2}.h^{-1}$ (Table 1). In solutions of calcium and magnesium chloride, no precipitates are generated; rather, aluminium electrodes get coated with a white film that is dense in the presence of Ca^{2+} and loose in the presence of Mg^{2+} [17,18]. Previous studies [14] have demonstrated that in aqueous electrolytes, Al oxidation occurs during an anodic pulse:

$$Al^0 \rightarrow Al^{3+} + 3e^- \qquad E_0 = -1.67 \text{ V (SHE)} \qquad (2)$$

In an aqueous electrolyte with a $pH > 3$, the Al^{3+} ion is going through a rapid hydrolysis process:

$$Al^{3+} + 3H_2O \rightarrow Al(OH)_3 + 3H^+ \qquad (3)$$

or

$$Al^{3+} + 2H_2O \rightarrow AlOOH + 3H^+ \qquad (4)$$

During the cathode pulse, only the hydrogen evolution reaction (5) occurs, as the standard reduction potential of the redox pair Al^{3+}/Al (equation 2) is markedly lower than the potential of the hydrogen evolution reaction (HER).

$$2H_2O + 2e^- \rightarrow H_2\uparrow + 2OH^- \qquad (5)$$

In Sr^{2+} and Ba^{2+} solutions, an identical pause potential of -1.18 V is attained after the pulses, as seen in Table 1, which is more positive than the standard potential of reaction (2). The electrode potentials during the interval after the cathodic pulse are -1.7 V and -1.5 V in the presence of Sr^{2+} and Ba^{2+}, respectively (Table 1). In Ca^{2+} and Mg^{2+} solutions, substantial potentials are generated during both anodic and cathodic pulses, which gradually decrease upon current end (Figure 1b), indicating the exceptionally high resistance of the developing passivation film on the aluminium surface, particularly in the presence of Ca^{2+} ions.

The chronopotentiograms of the aluminium electrode in the studied electrolytes demonstrated the development of a highly resistant passivating layer in Mg^{2+} and Ca^{2+} solutions, both under pulsed electrolysis and direct current conditions (Figure 1c). Upon the application of an anodic current density of 10 mA cm^{-2} to the aluminium electrode, a potential of -0.75 V was observed in all examined electrolytes. Upon transitioning from anodic to cathodic current, a transient period occurs, the length of which is determined by the cationic composition of the electrolyte. Lower potentials are observed in Mg^{2+} and Ca^{2+} solutions (-1.9 V; -1.6 V) compared to Sr^{2+} and Ba^{2+} solutions (-1.5 V; -1.4 V). The transition time for both groups of cations also differs: in the presence of activating ions Sr^{2+} and Ba^{2+} it is 5 s and more than 50 s in the presence of passivating ions Mg^{2+} and Ca^{2+} (Table 1).

The cyclic voltammograms of the aluminum electrode (Figure 2a) exhibit a distinct passivity region within the potential range of -1.2 V to -0.8 V in all investigated electrolytes. A considerable alteration in current values is observed at potentials above -0.8 V and falling below -1.2 V, indicating the occurrence of anodic oxidation of aluminium (1-3) and cathodic evolution of hydrogen (4). The electrical current values, and thus the rate of hydrogen evolution as per reaction (4), in Mg^{2+} and Ca^{2+} cation solutions are roughly an order of magnitude greater than those in Sr^{2+} and Ba^{2+} based electrolytes (Figure 2b). The application of an alternating pulsed current to the electrochemical system under investigation also influences the varying pH of the electrolyte (Table 1). The process of active hydrogen evolution reaction facilitates the alkalization of the electrolyte solution, achieving a pH of 10 in solutions containing Sr^{2+} and Ba^{2+} ions.

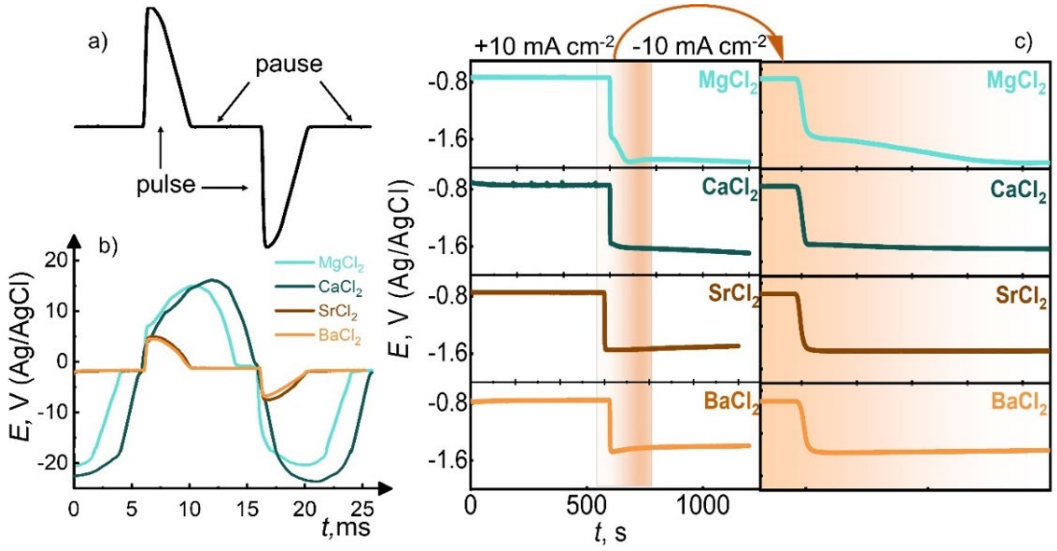

Figure 1. Current (a) and potential (b) profiles of aluminium electrode under pulse electrolysis conditions, and chronopotentiograms (c) of aluminium electrode in 1 mol.L^{-1} metal chloride solutions.

The Evans polarization corrosion diagrams plotted according to the Tafel equation distinctly illustrate that the passivity region of aluminium in Mg^{2+} and Ca^{2+} solutions is approximately 1.5 times broader than in Sr^{2+} and Ba^{2+} solutions (Figure 2b). The slope coefficients of the cathodic b_{cat} and anodic b_{an} linear sections that characterize the polarization resistances of the anodic and cathodic processes in the vicinity of the corrosion potential are near the theoretical values of 58 mV.dec^{-1} (as per the Nernst equation) in Mg^{2+} and Ca^{2+} solutions, while they are slightly lower in Sr^{2+} and Ba^{2+} solutions (Table 1). The corrosion potential E_{corr} of aluminium in Sr^{2+} and Ba^{2+} solutions is approximately -1.1 V. The presence of Mg^{2+} and Ca^{2+} results in a notable decrease, approximately -1.3 V (Table 1).

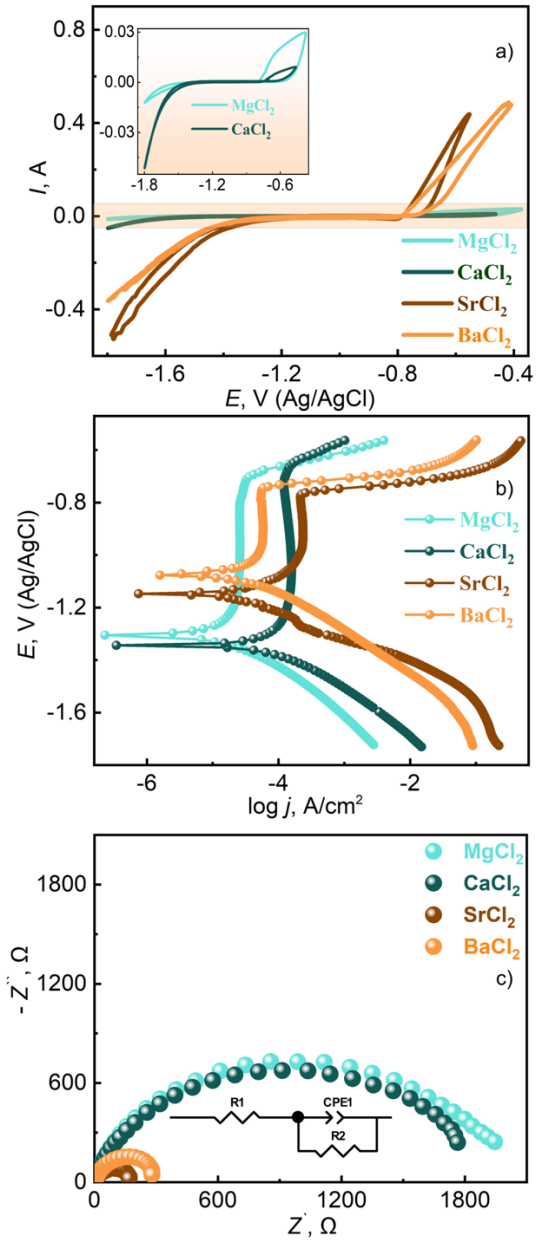

Figure 2. CVs at scan rate 5 mV.s^{-1} (a), Evans diagram at scan rate 5 mV.s^{-1} (b) and Impedance hodograph (c) of aluminium electrode in Cl^- containing electrolytes with a concentration of 1 mol.L^{-1}.

The corrosion current of aluminium, independently of the solution's composition, is $logj_{corr}$ = -5.8±0.1 mA.cm^{-2}. This is likely attributable to the impact of Cl^- anions. Chlorine anions, adsorbed on the passive oxide surface, provide an activating influence, facilitating its dissolution [13]. The aluminium electrode potential during anodic polarization at 0.75 V corroborates this, remaining unaffected by the cationic composition of the electrolyte (Figure 1b).

The results of electrode impedance measurements in comparable electrolyte solutions (Figure 2c) were converted into equivalent electrical circuits using the ZView equivalent circuit program (version 3.5i). The constant phase element (CPE), linked to the double-layer capacitance, resistance *R1*, is rather uniform over all electrolyte solutions at elevated frequencies, whereas *R2* represents the charge transfer resistance within the oxide layer (Table 1). This parameter greatly differs between the two groups of cations. The *R2* values for Mg^{2+} and Ca^{2+} demonstrate a significant barrier to charge transfer at the film surface. In Sr^{2+} and Ba^{2+} based electrolytes the barrier layer is absent, resulting in minimal charge transfer resistance.

XRD analyses of aluminium oxidation products under PAC conditions (Figure 3) revealed highly dispersed product formation in Sr^{2+} and Ba^{2+} solutions consist of a mixture of monoclinic aluminium oxyhydroxide phase (space group $P2_1/a$, JCPDS #21–1307) and aluminium hydroxide (space group *Cmcm*, JCPDS #01–072–0359) (Table 2). The AlOOH and $Al(OH)_3$ phases exhibited markedly different average particle sizes (D_{av}), with AlOOH being significantly smaller (1.9 and 2.2 nm) than $Al(OH)_3$ (20.4 and 13.9 nm) for Sr^{2+} and Ba^{2+} contenting electrolytes respectively.

In the presence of Mg^{2+} and Ca^{2+} cations, passivating films are formed on the aluminium surface, comprising two oxide phases: the

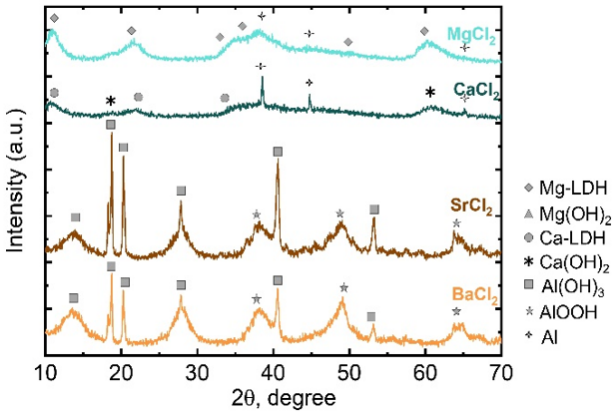

Figure 3. XRD patterns of the aluminium oxidation products formed under PAC conditions.

electrolyte metal hydroxides $Ca(OH)_2$ (portlandite, space group *P3m1*, ICDD 04-0733) or $Mg(OH)_2$ (brucite, space group *P3m1*, ICDD 07-0239) and layered double hydroxides (LDHs) [19-23] (see Table 3). The average crystallite sizes (D_{av}) and concentration of monophase hydroxides were 18 nm, 13 % and 25 nm, 33 % for $Mg(OH)_2$ and $Ca(OH)_2$ respectively (Table 2). The predominant phase in films formed on the aluminium electrode surface in electrolytes with Mg^{2+} or Ca^{2+} is layered double hydroxides (LDH), $[M_{1-x}^{2+}\ M_x^{3+}(OH)_2]^{x+}(\ A^{n-})_{x/n}mH_2O$ where M^{2+} represents any divalent metal cation, M^{3+} any trivalent metal cation and A^{n-} an anion (inorganic or organic), and x ranges from 0.15 to 0.33 and are known as anion-exchange clay materials. The concentrations of these LDHs are 87% and 67% for films formed using $MgCl_2$ and $CaCl_2$ electrolyte solutions, respectively.

Under PAC on the aluminium surface are formed *Mg-Al* LDH - Chloride hydrotalcite $Mg_6Al_2(OH)_{16}Cl_2{\cdot}4H_2O$ (space group *P3m*, ICDD 22-0700) or hydrocalumite *Ca-Al* LDH - $Ca_2Al(OH)_6Cl{\cdot}2H_2O$ (space group *P3c,* ICDD 42-0065) in Mg^{2+} and Ca^{2+} solutions respectively. The unit cell parameters of the trigonal and rhombohedral of these LDHs are presented in Table 2. The parameter a can be used to indirectly estimate the ratio of metals in LDH. In *Mg*-LDH, a = 3.05 Å, the ratio Mg:Al = 3:1. For *Ca*-LDHs, the value is almost twice as large, a = 5.74, which is typical of the hydrocalumite superstructure, where calcium ions occupy specific positions. This value of the parameter a indicates the ordering of cations in a ratio of Ca:Al = 2:1 [24]. The average particle size of these *Mg*-LDHs and *Ca*-LHDs are 18 and 25 nm, respectively.

Table 2. Results of the X-ray diffraction patterns refinement.

Cation electrolyte	Phase	Space group	Lattice parameter, Å	D_{av}, nm	Concentration, %
Mg^{2+}	$Mg_6Al_2(OH)_{16}Cl_2{\cdot}4H_2O$ hydrotalcite	*R3m*	a = 3.050 c = 23.025	15	87
	$Mg(OH)_2$ brucite	*R3m1*	a = 3.142 c = 4.766	18	13
Ca^{2+}	$Ca_2Al(OH)_6Cl{\cdot}2H_2O$ hydrocalumite	*P21*	a = 5.744 c = 23.268	16	67
	$Ca(OH)_2$ portlandite	*P3m1*	a = 3.585 c = 4.892	25	33
Sr^{2+}	AlOOH boehmite	*Cmcm*	a = 2.8191 b = 12.5853 c = 3.6799	1.9	80
	$Al(OH)_3$ gibbsite	*P2₁/a*	a = 5.0014 b = 8.6531 c = 4.6844 β = 90.9656	20.4	20
Ba^{2+}	AlOOH boehmite	*Cmcm*	a = 2.8093 b = 12.5564 c = 3.6727	2.2	86
	$Al(OH)_3$ gibbsite	*P2₁/a*	a = 5.0764 b = 8.6014 c = 4.6761 β = 90.9783	13.9	14

Table 3. Influence of reaction conditions on the electrochemical behavior of aluminum.

№	Current	Electrolyte	Phase	D_{av}, nm	Reference
1	Pulsed alternating current	$MgCl_2$ $CaCl_2$ $SrCl_2$ $BaCl_2$	Mg-Al LDH films Ca-Al LDH films AlOOH/$Al(OH)_3$ powder AlOOH/$Al(OH)_3$ powder	15 16 1.9/20.4 2.2/13.9	This article
2	direct current	$MgCl_2$ $Mg(NO_3)_2$	Mg-Al-LDH powder	4 9	[22]
3	direct current	NaCl	Mg-Al-LDH powder	65	[23]
4	alternating current	NaCl	AlOOH powder CuO powder	5000	[26]
5	direct current	NaCl	AlOOH powder $Al(OH)_3$ powder	50-200	[27]

It is established that the oxidation of metals under both direct and alternating current conditions typically results in the formation of dispersed metal oxides or hydroxides [25-27]. Zinc exhibits the formation of more complex structures in solutions containing potassium or magnesium cations [28]. The nature of electrolyte and current source could have a significant influence on the properties of the obtained products as shown in Table 3. Our observations indicate that when passivating metals like aluminium, the application of alternating polarization and the occurrence of cathodic processes result in the formation of passive layers predominantly composed of electrolyte cations, rather than cations of the electrode metal.

4. Conclusions

Studies of the electrochemical properties of aqueous electrolyte solutions of alkaline earth metal cations and chloride anions under pulsed electrolysis conditions revealed that electrochemical behavior depends on the nature of the electrolyte cation, which determines the direction of process development when the electrode polarity is periodically maintained. In chloride electrolytes with a cationic composition of Ba^{2+} or Sr^{2+} at a concentration of 1 mol/L, the application of a symmetrical alternating pulsed current leads to dispersion of the aluminum electrodes, resulting in the formation of a product consisting of a mixture of AlOOH and $Al(OH)_3$ phases. In Mg^{2+} and Ca^{2+} chloride solutions, the products of pulsed electrolysis are dense films consisting of magnesium hydroxides and hydrochlorides, as well as layered double hydroxides (LDHs) – hydrotalcite $Mg_6Al_2(OH)_{16}Cl_2{\cdot}4H_2O$ (*Mg-Al* LDH) and hydrocalumite $Ca_2Al(OH)_6Cl{\cdot}2H_2O$ (*Ca-Al* LDH). A combination of cyclic voltammetry, impedance spectroscopy, and chronopotentiometry showed that, despite the presence of Cl^- ions, Mg^{2+} and Ca^{2+} cations form passivating layers that inhibit generator formation processes even under pulsed electrolysis conditions. These results may represent a step forward in our fundamental understanding of the electrochemistry of valve metals under the influence of pulsed electric fields and open new approaches to the controlled formation of protective interphase boundaries.

Acknowledgment

The study was funded by Russian Science Foundation (no. 25-19-00280). The X-ray powder diffraction studies were carried out within the Platov South-Russian State Polytechnic University (NPI) using the equipment of Shared Research Center “Nanotechnologies”. The authors declare that they have no known financial conflicts of interest or personal relationships that could have influenced the work presented in this article.

CRedit Author Statement

Author Contributions: Marina Kubanova: Methodology, Investigation, Data curation. Tatyana Yureva: Investigation, Data curation. Elena Yatsenko: Investigation, Data curation. Yash V. Kataria: Investigation, Data curation. Alexandra Kuriganova: Writing – review & editing, Writing – original draft, Project administration, Methodology, Funding acquisition. Mikhail Lipkin: Writing – review & editing. Nina Smirnova: Writing – review & editing, Writing – original draft, Supervision, Conceptualization. All authors have read and agreed to the published version of the manuscript.

References

[1] Shih, A.J., Monteiro, M.C., Dattila, F., Pavesi, D., Philips, M., Da Silva, A.H., Koper, M.T. (2022). Water electrolysis. *Nature Reviews Methods Primers*, *2*(1), 84. DOI: 10.1038/s43586-022-00164-0.

[2] Lasia, A. (2019). Mechanism and kinetics of the hydrogen evolution reaction. *International Journal of Hydrogen Energy*, *44*(36), 19484-19518. DOI: 10.1016/j.ijhydene.2019.05.183.

[3] Zhang, H., Liu, X., Li, H., Hasa, I., Passerini, S. (2021). Challenges and strategies for high-energy aqueous electrolyte rechargeable batteries. *Angewandte Chemie International Edition*, *60*(2), 598-616. DOI: 10.1002/anie.202004433.

[4] Chen, S., Zhang, M., Zou, P., Sun, B., Tao, S. (2022). Historical development and novel concepts on electrolytes for aqueous rechargeable batteries. *Energy & Environmental Science*, *15*(5), 1805-1839. DOI: 10.1039/D2EE00004K.

[5] Smith, L., Dunn, B. (2015). Opening the window for aqueous electrolytes. *Science*, *350*(6263), 918-918. DOI: 10.1126/science.aad5575.

[6] Dubouis, N., Grimaud, A. (2019). The hydrogen evolution reaction: from material to interfacial descriptors. *Chemical Science*, *10*(40), 9165-9181. DOI: 10.1039/C9SC03831K.

[7] Yokoyama, Y., Fukutsuka, T., Miyazaki, K., Abe, T. (2018). Origin of the electrochemical stability of aqueous concentrated electrolyte solutions. *Journal of The Electrochemical Society*, *165*(14), A3299-A3303. DOI: 10.1149/2.0491814jes.

[8] Kuriganova, A., Kubanova, M., Leontyev, I., Molodtsova, T., Smirnova, N. (2022). Pulse electrolysis technique for preparation of bimetal tin-containing electrocatalytic materials. *Catalysts*, *12*(11), 1444. DOI: 10.3390/catal12111444.

[9] Molodtsova, T., Ulyankina, A., Gorshenkov, M., Kubrin, S., Kaichev, V., Smirnova, N. (2024). High-throughput electrochemical strategy for synthesis of iron-based nanostructures for electrocatalytic water splitting. *Journal of Materials Science*, *59*(4), 1265-1279. DOI: 10.1007/s10853-023-09290-w.

[10] Kuriganova, A., Leontyev, I., Smirnova, N. (2024). Electrochemistry of Pt and Pd Under Pulse Electrolysis Conditions. *Journal of The Electrochemical Society*, *171*(12), 126505. DOI: 10.1149/1945-7111/ad9b51.

[11] Kuriganova, A.B., Brink, I.Y., Smirnova, N.V. (2024). Theoretical and technological fundamentals of pulse electrolysis for the production of electro-and catalytically active materials based on Pt, Pd, Sn and graphene nanostructures. *Nano Materials Science*. DOI: 10.1016/j.nanoms.2024.09.007.

[12] Kuriganova, A., Smirnova, N. (2025). New Insights into Controlling the Functional Properties of Tin Oxide-Based Materials. *Journal of Electrochemistry*, *31*(1), 2. DOI: 10.61558/2993-074X.3509.

[13] Natishan, P.M., O'Grady, W.E. (2014). Chloride ion interactions with oxide-covered aluminum leading to pitting corrosion: a review. *Journal of the Electrochemical Society*, *161*(9), C421-C432. DOI: 10.1149/2.1011409jes.

[14] Kubanova, M., Kuriganova, A., Leontyev, I., Gorshenkov, M., Kolesnikov, E., Yatsenko, A., Smirnova, N. (2025). Pulse electrolysis modes in the synthesis of dispersed aluminium oxides and hydroxides. *Electrochimica Acta*, 147638. DOI: 10.1016/j.electacta.2025.147638.

[15] Amri, A., Fithri, N.A., Said, M., Lesbani, A. (2026). Green-Modified Ni/Al LDH with Camellia sinensis Bioactives: A Sustainable Strategy for Ceftriaxone Removal. *Bulletin of Chemical Reaction Engineering & Catalysis*, *21*(1), 96-111. DOI: 10.9767/bcrec.20513.

[16] Ota, K.I. (2014). *Encyclopedia of applied electrochemistry*. G. Kreysa, R.F. Savinell (Eds.). New York: Springer. DOI: 10.1007/SpringerReference_303978.

[17] Collazo, A., Nóvoa, X.R., Pérez, C. (2014). The role of Mg2+ ions in the corrosion behaviour of AA2024-T3 aluminium alloys immersed in chloride-containing environments. *Electrochimica Acta*, *124*, 17-26. DOI: 10.1016/j.electacta.2013.10.130

[18] Di Liberto, G., Maleki, F., Pacchioni, G. (2022). pH dependence of MgO, TiO2, and γ-Al2O3 surface chemistry from first principles. *The Journal of Physical Chemistry C*, *126*(24), 10216-10223. DOI: 10.1021/acs.jpcc.2c02289.

[19] Altalhi, A.A., Mohamed, E.A., Negm, N.A. (2024). Recent advances in layered double hydroxide (LDH)-based materials: fabrication, modification strategies, characterization, promising environmental catalytic applications, and prospective aspects. *Energy Advances*, *3*(9), 2136-2151. DOI: 10.1039/D4YA00272E.

[20] Cristoforetti, A., Harare, M.T., Fedel, M. (2026). Hydrothermal vs. electrochemical synthesis of CaAl-layered double hydroxides smart pigments for steel corrosion protection. *Applied Clay Science*, *279*, 108045. DOI: 10.1016/j.clay.2025.108045.

[21] Khan, A.I., O'Hare, D. (2002). Intercalation chemistry of layered double hydroxides: recent developments and applications. *Journal of Materials Chemistry*, *12*(11), 3191-3198. DOI: 10.1039/b204076j.

[22] Ouarghi, A., Zaidi, S., Chaabane, T., Fernandes, A., Darchen, A., Omine, K., Sivasankar, V. (2025). Magnesium–Aluminium–layered double hydroxides (Mg–Al–LDH) by MgCl2/Mg (NO3) 2 mediated electrolysis using aluminium/vitreous carbon electrodes: Prominent in removing fluoride and nitrate from semiconductor wastewater. *Journal of the Indian Chemical Society*, 102281. DOI: 10.1016/j.jics.2025.102281

[23] Molano-Mendoza, M., Donneys-Victoria, D., Marriaga-Cabrales, N., Mueses, M.A., Puma, G. L., Machuca-Martínez, F. (2018). Synthesis of Mg-Al layered double hydroxides by electrocoagulation. *MethodsX*, *5*, 915-923. DOI: 10.1016/j.mex.2018.07.019

[24] Gevers, B.R., Labuschagné, F.J. (2020). Green synthesis of hydrocalumite (CaAl-OH-LDH) from Ca(OH)2 and Al(OH)3 and the parameters that influence its formation and speciation. *Crystals*, *10*(8), 672. DOI: 10.3390/cryst10080672.

[25] Anicai, L., Petica, A., Patroi, D., Marinescu, V., Prioteasa, P., Costovici, S. (2015). Electrochemical synthesis of nanosized TiO2 nanopowder involving choline chloride based ionic liquids. *Materials Science and Engineering: B*, *199*, 87-95. DOI: 10.1016/j.mseb.2015.05.005.

[26] Usoltseva, N.V., Korobochkin, V.V., Balmashnov, M.A., Dolinina, A.S. (2014). Characterization of copper and aluminum AC electrochemical oxidation products. *Procedia Chemistry*, *10*, 320-325. DOI: 10.1016/j.proche.2014.10.054.

[27] Petrova, E.V., Dresvyannikov, A.F., Khairullina, A.I., Mezhevich, Z.V. (2019). Physicochemical properties of alumina synthesized with electrogenerated reagents. *Russian Journal of Physical Chemistry A*, *93*(7), 1399-1405. DOI: 10.1134/s0044453719070227.

[28] Ulyankina, A., Tsarenko, A., Yatsenko, A., Gorshenkov, M., Smirnova, N. (2023). Photo (electro) catalytic Performance of ZnO-Based Nanopowders Prepared through Pulse Alternating Current Electrosynthesis in Alkaline Earth Chloride Electrolytes. *ChemistrySelect*, *8*(37), e202300457. DOI: 10.1002/slct.202300457.